Size-Dependent Valence and Conduction Band-Edge Energies of Semiconductor Nanocrystals

Jacek Jasieniak,[†,*] Marco Califano,[‡] and Scott E. Watkins[†]

[†]Materials Science and Engineering, CSIRO, Bayview Avenue, Clayton, Victoria, 3168, Australia, and [‡]School of Electronic and Electrical Engineering, University of Leeds, Leeds, L2S 9JT, United Kingdom

ABSTRACT Through the use of photoelectron spectroscopy in air (PESA), we investigate the size-dependent valence and conduction band-edge energies of CdSe, CdTe, PbS, and PbSe semiconductor quantum dots (QDs). The results are compared to those of previous studies, based on differing experimental methods, and to theoretical calculations based on k·p theory and state-of-the-art atomistic semiempirical pseudopotential modeling. To accurately map out the energy level landscapes of QDs as a function of size, the QDs must be passivated by comparable surface chemistries. This is highlighted by studying the effect of surface chemistry on the valence band-edge energy in an ensemble of 4.7 nm CdSe QDs. An energy level shift as large as 0.35 eV is observed for this system through modification of surface chemistry alone. This shift is significantly larger than the size-dependent valence band-edge shift that is observed when comparable surface chemistries are used.

KEYWORDS: nanocrystal · quantum dot · energy level · ionization energy · electron affinity

When the radius of a semiconductor nanocrystal is reduced to dimensions below its effective exciton Bohr radius (a_b), exciton confinement results in the evolution of discrete optical transitions that gradually shift to higher energies with decreasing size.[1] Provided that the size distribution of an ensemble of such nanocrystals is narrow and that the overlap between different transitions is sufficiently small, the discrete optical features which result provide information on mean particle size,[2] ensemble distribution width,[3] particle concentration,[4,5] and the electronic structure within the conduction and valence bands.[6,7] With progressive improvements in the synthetic protocols to achieve nearly monodisperse ensembles of semiconductor colloids, the confinement effects in numerous semiconductors, of a variety of shapes, have already been reported.[8−11] Of all the explored semiconductors, CdSe, CdTe, PbS, and PbSe QD systems have shown the most promise, with application in 3rd generation solar cells,[12−14] as photodetectors,[15] and in light-emitting diodes.[16]

While optical absorption measurements yield information on the QD size and the relative energy level configurations, they do not allow for the determination of the absolute energy level position with respect to a standard potential. This understanding is vital to unearthing a more complete picture of the confinement effect in a given system. Theoretical predictions based on effective mass approximations (EMA),[17] tight-binding (TB),[18] charge patching (CP),[19] and semiempirical pseudopotential (SEMP)[20] models have predicted varying size dependencies of the ionization and electron affinities for semiconductor nanocrystals. Studies on CdSe nanocrystals have shown that the most primitive of these models, EMA, consistently overestimates the valence and conduction band size-dependent shifts because it unrealistically assumes an infinite potential barrier at the dot surface, yielding a $1/R^2$ scaling with size.[21,22] Better agreement has been found for the more sophisticated TB, CP, and SEMP models.

To date, the most common methods for the determination of the size-dependent conduction and/or valence band-edge shift in quantum confined systems have been cyclic voltammetry (CV), ultraviolet photoelectron spectroscopy (UPS), and X-ray absorption spectroscopy (XAS).[22−27] The most popular of these has been UPS, because it can map out the entire valence band structure, including the band-edge and surface state contributions of a material.[28] Recent studies on the work-function of indium tin oxide (ITO), have shown that shifts of up to 0.5 eV are observed due to the exposure of the sample to high intensity UV radiation.[29] This suggests that the high intensity and presumably the high energies (typically He I radiation at 21.2 eV) of the ultraviolet radiation used in conventional UPS measurements may induce artifacts that will affect

* Address correspondence to Jacek.Jasieniak@csiro.au.

Received for review May 9, 2011 and accepted June 12, 2011.

Published online June 12, 2011
10.1021/nn201681s

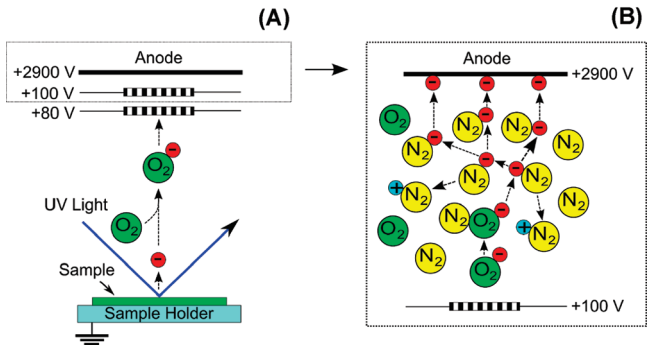

Figure 1. (A) A schematic of the PESA measurement. (B) A depiction of the electron avalanche process that takes place within the high voltage gradient chamber allowing for high sensitivity of photoelectron detection from the sample.

the determination of the true valence band-edge. A complementary technique to UPS is XAS. It utilizes synchrotron radiation to directly probe vacant states within the conduction band.[26] By using UPS in conjunction with XAS, a complete mapping of the electronic structure in any material can be made. Of all three methods, cyclic voltammetry is the most convenient because it is performed under ambient conditions and directly on electro-active species in solution or as thin-films. However, the accuracy of the experiments can be difficult to estimate, partly because for each system careful consideration of the solvent, the electrolyte, and the electrodes must be taken.[30] Each method therefore has certain advantages and disadvantages, and may comparatively result in a variation of the determined electronic structure.

Recent studies on nanocrystal energy level structures have unveiled a phenomenon that transcends the nature of the measurement—the electronic structure of nanocrystallites is inherently coupled to their surface chemistry.[23,27,31,32] The group of Guyot-Sionnest was one of the first to demonstrate this effect using CV to show that the reduction potential of 7.0 nm CdSe nanocrystals with TOPO ligands was less negative than those overcoated with octanethiol.[23] In an extension to this work, Soreni-Harari *et al.* also used electrochemical means to study the influence of surface chemistry on the electronic structure of InAs nanocrystals of a given size; variations to the valence band energy of up to 0.4 eV were observed.[31] This work suggested that the energy level variations did not result from a surface ligand dipole effect and were instead directly correlated to the surface binding moiety on the ligands. While both of these studies looked at a single nanocrystal size, Wu *et al.* used XPS and UPS to show that CdSe with hexadecylamine/tri-*n*-octylphosphine oxide surface chemistries exhibited a vastly different size-dependent valence band shift compared to those with pyridine surfaces coatings.[32] It was suggested that the finite lifetime of the residual hole following photoionization within the nanocrystal was responsible for these effects. Each of these preliminary studies highlights the importance of surface chemistry in defining the size-dependent energy level structure of quantum confined nanocrystals.

The drastic effect of ligands on the energy level structure of nanocrystals does create some concern when using ultrahigh-vacuum (UHV) based techniques (*e.g.*, UPS, XPS, and XAS) because the surface chemistry can be modified through desorption.[27] CV is therefore an attractive alternative because it can be performed on nanocrystals with their surface chemistries intact. In this study, we utilize another method, namely photoelectron emission spectroscopy in air (PESA) to determine the size-dependence of the ionization energy of CdSe, CdTe, PbS, and PbSe QDs. With surface chemistry having such potentially drastic effects on the energy levels, we also employ PESA to investigate how different surface ligands influence the ionization energy in the case of CdSe nanocrystals. Advantageously, PESA is a rapid and reproducible measurement, that is performed on thin films under ambient conditions. This type of photoelectron spectroscopy has been previously used to determine the ionization potentials of a number of semiconductors[33] and metals,[34] as well as the highest occupied molecular orbital in numerous organic materials.[35−37] It has not, however, been applied to the study of the ionization potential of semiconductor QDs as a function of size. Before proceeding to illustrate the effects of ligands on CdSe nanocrystals and the energy level configurations of the various QDs studied here, we begin with a brief introduction to the basics of PESA and an overview of the electronic structure of quantum confined nanocrystals.

Photoemission Spectroscopy in Air. A schematic of the PESA measurement is shown in Figure 1A. In this type of spectroscopy, the incident radiation is scanned across a range of energies (3.4−6.4 eV) which permits available electrons to be photoemitted from the sample through the photoelectric effect. An electron that has been photoemitted from its ground state is accelerated away from the sample by a weak positive bias (sample is at 0 V) and in the process is picked up by an oxygen molecule in air. The singlet oxygen radical anion continues to accelerate away from the sample and subsequently enters a high voltage gradient

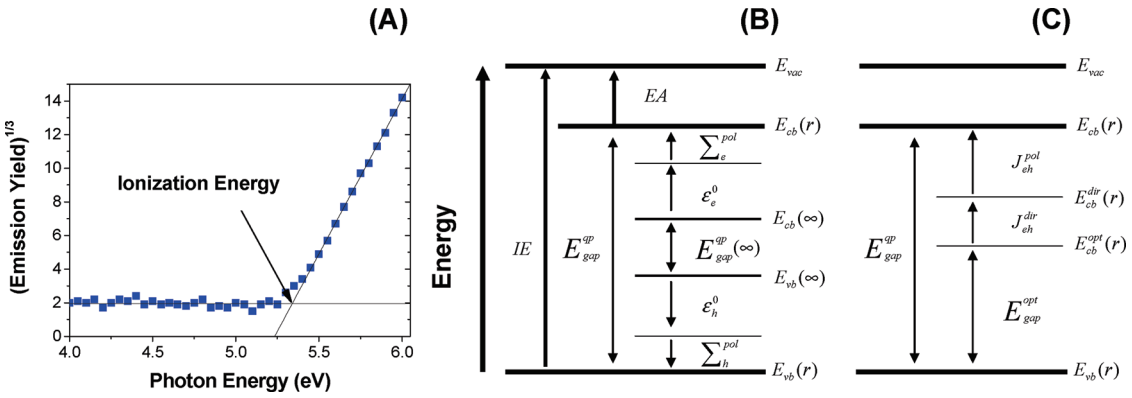

Figure 2. (A) A typical PESA spectrum showing the dependence of the cubic root on the photoelectron yield as a function of energy for the photoelectron signal at energies higher than the ionization energy. (B) A schematic of the electronic structure which exists in a semiconductor quantum dot. The ionization energy (IE) and electron affinity (EA) are given with reference to the vacuum energy (E_{vac}). The quasiparticle band gap (E_{gap}^{qp}), which correlates the IE to the EA through EA = IE − E_{gap}^{qp}, is broken up into its individual contributions. These contributions arise from electron (e) and hole (h) quantum (ε^0) and dielectric (Σ^{pol}) confinement terms. The bulk valence ($E_{vb}(\infty)$) and conduction ($E_{cb}(\infty)$) band-edge energies are also depicted. (C) The equivalent electronic structure of a quantum dot when determined directly from the known optical band gap (E_{gap}^{opt}), the direct Coulomb interaction (J_{eh}^{dir}) and the dielectric polarization (J_{eh}^{pol}) contribution. In this case, the energy levels are presented such that the determination of the E_{cb} is made from a known E_{vb}.

chamber which causes an electron avalanche to occur through an electron cascading process involving nitrogen gas (see Figure 1B). The free electrons involved in this avalanche process are detected at the anode and through calibration are correlated to the photoelectron yield (*Y*) of the sample. Macroscopic charging of the sample is minimized by using very weak UV intensities (4−400 nW/cm^2) for photoemission and by depositing materials as thin films on conductive substrates which are subsequently grounded during measurements. We have found that ITO-coated glass and even standard borosilicate glass are appropriate, but quartz is not sufficiently conductive.

The PESA measurement offers a simple means to the determination of a material's ionization energy; however, the samples do need to be exposed to air. Evidently, for samples which oxidize rapidly or can be contaminated by air-bound hydrocarbons and water, the measured photoionization energy can be significantly altered as a result. In the case of aluminum metal for example, photoelectron spectroscopy measurements in ultrahigh vacuum show that aluminum has a work function of 4.2 eV.[38] With the surface of an aluminum film oxidizing almost immediately in air, our own measurements of evaporated aluminum using PESA show that the work function ranges between 3.6 and 4.1 eV depending on sample history. The differences can be accounted for by stress-induced changes to the local density of states at the surface of aluminum caused by oxidation and adsorption of water.[34] In contrast, the QD samples studied here are typically prepared and handled under ambient conditions. This makes PESA a useful technique for studying their electronic structure.

Energy Level Structure in Quantum Dots. Photoelectron emission spectroscopy measures the yield of photoemitted electrons (*Y*) being ejected from a sample as a function of spectral energy. The threshold energy required for photoelectron emission is termed the photoionization threshold (see Figure 2A). It corresponds to the ionization energy (IE) of a material.[39] To determine the IE from photoelectron emission measurements, the spectrally dependent photoelectron emission yield must be interpreted through an appropriate model of the photoemission process.[40] In bulk semiconductors, the two most common photoelectron emission states arise from the valence band within the space-charge or flat-band potential spatial regions and from the surface. In QDs, where band-bending does not occur and a high surface-to-volume ratio exists, it is most likely that photoemission occurs from the size-dependent valence band states with a surface scattering contribution. The empirical functional form of this photoemission process is given by[41]

$$Y \propto (E - \mathrm{IE})^3 \quad (1)$$

where *E* is the energy of the incident light. In Figure 2A the cubic root of the photoelectron yield of a representative PESA measurement of 5.1 nm CdSe QDs is shown. The IE is determined from the intercept to be 5.33 eV. Despite the origins of the cube root fit to the photoelectron yield stemming from bulk semiconductor physics, it appears that eq 1 remains valid for semiconductor nanocrystals. Notably, the use of a square root dependence, which is common for metals[34] and organic semiconductors,[35] provides only a slightly worse fit, which in any case does not greatly influence the extrapolated IE (see Supporting Information).

For semiconductors and insulators, one can further determine the electron affinity (EA) from the IE by considering that EA = IE − E_{gap}^{qp}, where E_{gap}^{qp} is the

quasiparticle band gap. E_{gap}^{qp} is equivalent to the formation energy of a noninteracting electron−hole pair and is commonly termed the electronic transport gap. Adopting a similar notation to that proposed by Franceschetti and Zunger,[42] E_{gap}^{qp} can be decomposed into individual electron (e) and hole (h) quantum (ε^0) and dielectric (Σ^{pol}) confinement terms through

$$E_{gap}^{qp} = E_{gap}^{qp}(\infty) + \varepsilon_e^0 + \Sigma_e^{pol} + \varepsilon_h^0 + \Sigma_h^{pol} = E_{gap}^0 + \Sigma_e^{pol} + \Sigma_h^{pol} \quad (2)$$

where $E_{gap}^{qp}(\infty)$ is the bulk quasiparticle band gap and E_{gap}^0 is the single-particle gap of the QD and includes only the size quantization effects. A schematic of the energy level structure based on all these parameters is shown in Figure 2B. If the zero energy reference is that of the vacuum level (E_{vac}), then the energies of the individual levels are negative. Thus, the valence band-edge (E_{vb}) and conduction band-edge (E_{cb}) energies are given as −IE and −EA, respectively.

The E_{gap}^{qp} can be measured directly from charging experiments using scanning tunnelling microscopy or cyclic voltammetry.[22,43] These experiments can be difficult and time-consuming, thus an easier method is to theoretically approximate it from a known E_{vb} or E_{cb} and the optical band gap E_{gap}^{opt} as measured *via* absorption spectroscopy.

The optical band gap is related to the quasiparticle band gap through

$$E_{gap}^{opt} = E_{gap}^{qp} - J_{eh}^{dir} - J_{eh}^{pol} \quad (3)$$

where J_{eh}^{dir} is the direct Coulomb interaction between a confined electron−hole pair and J_{eh}^{pol} is the polarization energy, which arises from the interaction of one carrier with the image charge of the other across the dielectric discontinuity at the QD−matrix interface. Through the use of eq 3 the EA can be rewritten in terms of the optical band gap:

$$EA = IE - (E_{gap}^{opt} + J_{eh}^{dir} + J_{eh}^{pol}) \quad (4)$$

In Figure 2C we show the equivalent energy level diagram representing the determination of the EA through the use of the optical band gap, the direct Coulomb interaction, and the polarization contribution. Included, are the energies of the levels with contributions of only E_{gap}^{opt}, $E_{gap}^{opt} + J_{eh}^{dir}$, and $E_{gap}^{opt} + J_{eh}^{dir} + J_{eh}^{pol}$ to eq 4. These are depicted as E_{cb}^{opt}, E_{cb}^{dir} and E_{cb}, respectively.

The effects of direct and polarization induced Coulomb interactions on the electrons and holes in quantum dots were first considered by Brus under an effective mass approximation.[17,44] The expressions that were derived for J_{eh}^{dir} and J_{eh}^{pol} in that work can be applied here to provide an analytical approximation of eq 4.

$$EA \simeq IE - E_{gap}^{opt} - 1.786\frac{e^2}{4\pi\varepsilon_{QD}\varepsilon_0 R} - \frac{e^2}{4\pi\varepsilon_0 R}\left(\frac{1}{\varepsilon_M} - \frac{1}{\varepsilon_{QD}}\right) \quad (5)$$

where e is the elementary charge (C), ε_0 is the vacuum permittivity (F/m), $\varepsilon_{QD(M)}$ is the dielectric constant of the QD (matrix), and R is the nanocrystal radius. This expression can be used to approximate the EA from a known IE (or vice versa) and the experimentally determined optical band gap. Under this approximation, the problem reduces down to the correct choice of the dielectric constant for the matrix and the quantum dots.

The ligands which were adsorbed onto the different nanocrystals used here possess a dielectric constant of ~2. For this reason, we used this as an approximation to the dielectric constant of the host matrix. Although this has been a popular choice in the literature,[45] it is still unclear whether it is the ligand shell, the external surrounding environment or a combination of both that determines the QD's dielectric environment. Regarding the dielectric constants of the quantum dots, numerous studies have suggested that they should exhibit a size-dependence. Alves-Santos and co-workers recently used a Kramers−Kronig transformation of experimentally measured absorption coefficient data to show that CdS and CdSe nanocrystals do indeed exhibit size-dependent dielectric values, and their magnitude are consistent with the conventionally applied modified Penn-model;[46] for synthetically achievable sizes, the dielectric constants of these two semiconductors are found to be within ~20% of the bulk value. Using a similar approach, Moreels and co-workers found that for lead chalcogenide nanocrystals the size-dependence is much smaller than first thought.[47] It was suggested that this observation was due to the enhancement of the dielectric constant at the surface. Overall, based on the results of both of these studies, a relatively small size-dependent change of the dielectric constant for the semiconductors studied here is expected. Therefore, in this work we choose to adopt size-independent dielectric constants. In addition, as the kinetic energies of the electron and holes for all QDs are up to several tenths of an electronvolt (~50 THz), optical dielectric constants are used.

RESULTS AND DISCUSSION

The size-dependent evolution of the absorption features exhibited by ensembles of CdSe, CdTe, PbS, and PbSe quantum dots dispersed in chloroform are shown in Figure 3. The discrete optical transitions which are observed in each case indicate the narrow polydispersity of the various QD ensembles. From established calibration curves, one can easily and accurately

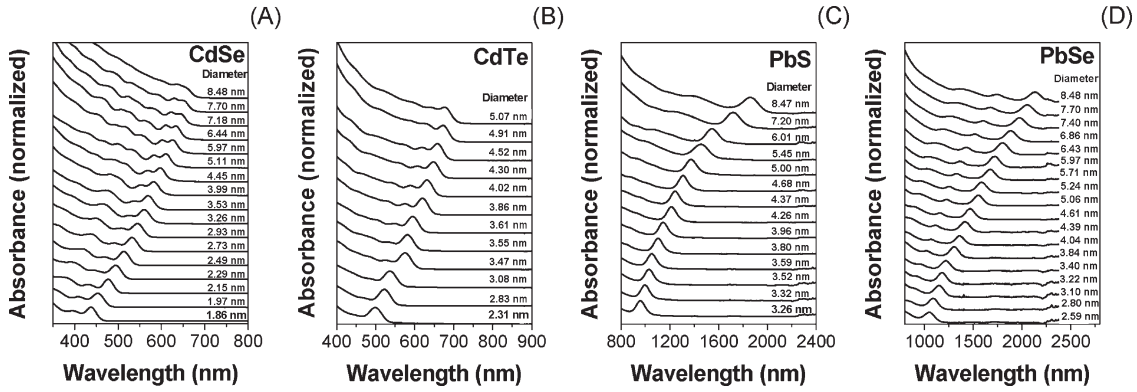

Figure 3. The size-dependent absorption spectra of (A) CdSe, (B) CdTe, (C) PbS, and (D) PbSe quantum dots.

determine particle size directly from the 1st absorption peak maxima.[2,4,48,49] For many electronic applications it is vital to also know the energy level diagram of these quantum dots. While a number of studies have attempted to address this issue, there still remains much uncertainty in these measurements.[22,25,26] The goal of this manuscript is to map out the size-dependent energy levels of these nanocrystals relative to vacuum using PESA. Before proceeding to these measurements, it is important to first understand how the surface chemistry influences the measured energy levels for a quantum dot of a given size.

Ligand Effects on Ionization Energy of CdSe Quantum Dots. It has recently been reported that InP QDs exhibit a large variation in their ionization energy and electron affinity following changes to their surface capping ligands.[31] In light of these observations, here we study the effects of pyridine, oleic acid, oleylamine, tri-*n*-octylphosphine oxide (TOPO) and dodecanethiol surface ligands on the ionization energy of an ensemble of 4.7 nm CdSe QDs. Before proceeding to these measurements, we focus on understanding the nature of each surface chemistry following ligand exchange.

The surface chemistry of the CdSe nanocrystals studied here was modified through a two-step process, involving (i) an initial pyridine exchange and (ii) a subsequent re-exchange with the intended ligand. The nature of the surface chemistry at each step was investigated through attenuated total reflectance Fourier transform infrared (ATR-FTIR) spectroscopy with all results being presented in Figure 4. We begin our analysis with pyridine-passivated CdSe nanocrystals.

The IR spectra of pyridine and pyridine surface-passivated CdSe nanoparticles are shown in Figure 4A. With guidance from previous works on the assignment of IR active resonances in pyridine[50−52] it can be qualitatively observed that pyridine passivates the majority of surface sites on the nanocrystals. The residual aliphatic stretches in the 2700−3000 cm^{-1} region do, however, show that our pyridine exchange protocols do not quantitatively displace the original aliphatic surface ligands. This finding is in agreement with Bowen Katari *et al.*,[53] who found that pyridine exchange of TOPO-coated CdSe nanocrystals was incomplete, with ~12% of the original TOPO ligands being retained.

Interest in pyridine as a coordinating species of metal and metal oxide surfaces has arisen because of the numerous coordination mechanisms that it presents.[54] To probe the binding mechanism of pyridine on CdSe nanocrystals in more detail we focus our attention on the 1400−1650 cm^{-1} IR region (see inset of Figure 4A). Analogous to previous studies of pyridine adsorbed onto metal sites,[54,55] the 1579 cm^{-1} (ν_{8a}) and 1436 cm^{-1} (ν_{19b}) bands of pyridine are shifted to higher wavenumbers following adsorption. The concordant development of the IR transitions between 1452 and 1472 cm^{-1} are indicative of pyridine coordinating directly to metal surface states.[56] Interestingly, the broad and weak bands centered at 1631 and 1550 cm^{-1} are not related to pyridine directly coordinating the metal-based Lewis acid sites, but to coordination of the surface through pyridinium.[56] This type of binding mechanisms is common for metal oxide surfaces, where surface hydroxyl groups can be deprotonated by the pyridine. The presence of OH stretches in the 3000−3700 cm^{-1} IR region supports the existence of hydroxyl groups in the sample. A likely scenario in this case is that surface adsorbed water is deprotonated by the pyridine to form pyridinium and metal hydroxides. The pyridinium can then in principle actively adsorb to naturally formed oxide, metal hydroxide, or bare selenium surface sites.

The labile nature of pyridine on CdSe surfaces is well documented.[57] For these surface studies, we exploited this property by actively repassivating the surface with our intended ligands. Beginning with oleic acid, from the IR spectra there is a clear indication of oleate passivation (Figure 4B). As previously seen for cobalt nanocrystals passivated with oleic acid[58] and through comparison with cadmium acetate dihydrate, the existence of the asymmetric and symmetric stretches of the carboxylate moiety at 1532 and 1410 cm^{-1}, respectively, indicate chemisorbed carboxylate functionalities.

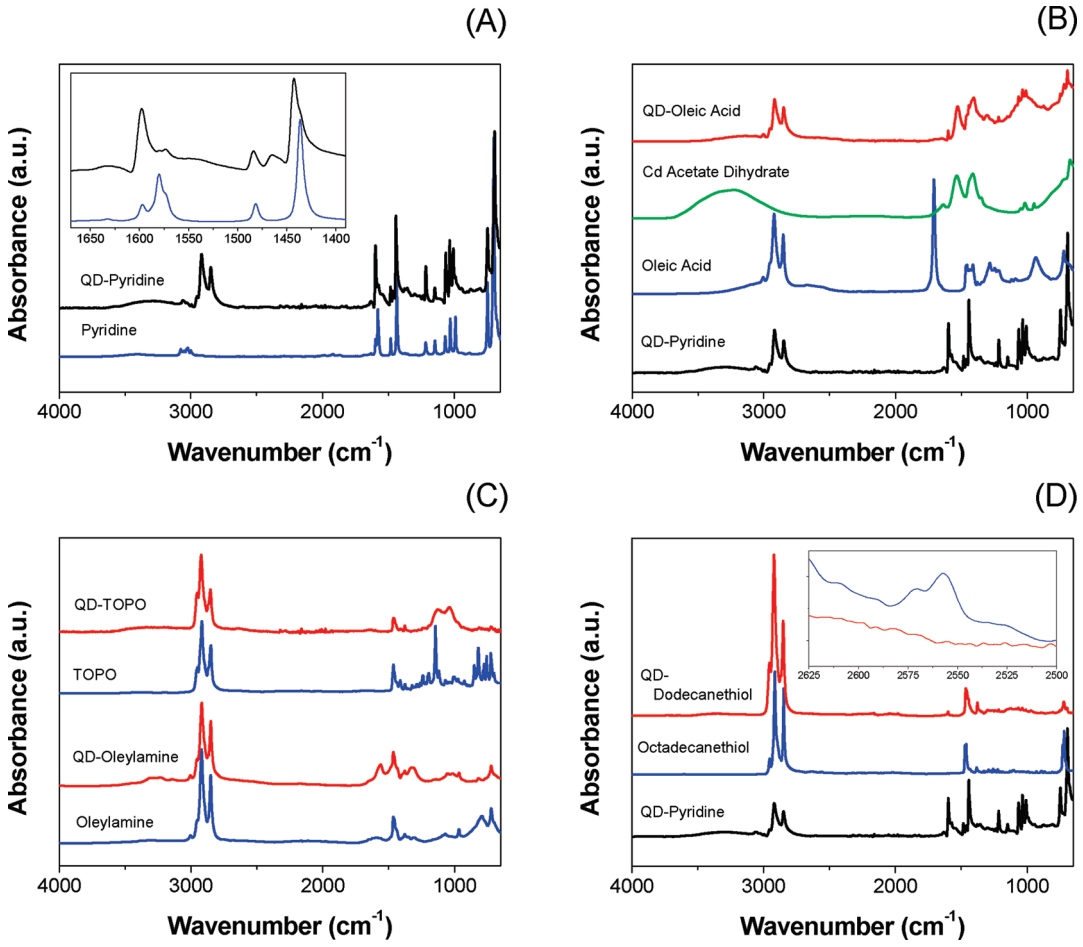

Figure 4. The ATR-FTIR spectra of CdSe quantum dots passivated with pyridine (A), oleic acid (B), oleylamine (C), tri-*n*-octylphosphine oxide (C), and dodecanethiol (D). In each of the plots the corresponding ligand IR absorption is shown, and where relevant, the spectrum of pyridine-coated quantum dots is also included. The IR spectra of CdSe with pyridine and dodecanethiol ligands possess an additional inset showing a magnified spectral region of the pyridine and the thiol signatures, respectively.

The lack of C═O (1710 cm^{-1}), C—O (1285 cm^{-1}), and out-of-plane O—H (937 cm^{-1}) signatures, as observed for oleic acid, indicate that the free acid does not exist at the surface and that the oxygen species of the carboxylate are symmetrically coordinating to the Cd surface states. Interestingly, despite the labile nature of the pyridine ligands, residual pyridine remains coordinated to the surface. This indicates that pyridine must bind to inaccessible sites on the surface compared to the oleate, or the relatively small binding energies of fatty carboxylates to the surface of CdSe prevents complete exchange.[59]

In contrast to oleate passivated CdSe, the adsorption of oleylamine on the surface is found to quantitatively displace pyridine (Figure 4C). This can be understood by the significantly higher binding constant of fatty amines compared to pyridine on CdSe surfaces.[57,59] In addition to the expected aliphatic resonances across the spectral region, the oleylamine shows evidence of N—H stretches arising from the $-NH_2$ functional groups centered at 3280 cm^{-1}, $-NH_2$ scissoring centered at 1590 cm^{-1}, C—N stretching at 1070 cm^{-1}, and $-NH_2$ bending at 791 cm^{-1}.[61] Upon adsorption onto CdSe, the IR spectrum closely resembles that of neat oleylamine, with additional new resonances developing at 1560, 1320, and 1017 cm^{-1}. The existence of N—H stretches clearly proves that the N—H group is retained following chemisorption. The resonance at 1560 cm^{-1}, which is believed to arise from the scissoring of an adsorbed amine,[60] further confirms that binding occurs to the surface through the amine group. The two other remaining resonances cannot at present be assigned, but due to the known sensitivity of the various stretches, bends, and scissoring actions of the amine group to local bonding, they are expected to arise from adsorbed amine species on the CdSe surface.[60] Early vibrational studies on cadmium halides complexes with aromatic amine adducts indeed confirm that vibrational modes at the spectral locations of each of the unidentified modes are observed.[62] Furthermore, the apparent shift of the $-NH_2$ bending modes originally centered at 791 cm^{-1},

TABLE 1. The Ionization Energy Dependence of 4.7 nm CdSe QDs on Surface Ligand

surface ligand	IE (eV)
alkyl amines[a]	5.40
trioctylphosphine oxide	5.45
oleic acid	5.60
alkane thiols[a]	5.65
pyridine	5.75

[a] Performed on alkyl chain lengths ranging from butyl to octadecyl.

may at least in part account for their existence. For completeness, the existence of pyridinium on the surface suggests that alkyl ammonium should be equally likely to form. Indeed, the asymmetric and symmetric stretches of the alkyl ammonium species have been observed at 1630 and 1550 cm^{-1}, respectively, which overlap with the $-NH_2$ scissoring modes.[63] Thus, based on this factor, we cannot rule out the existence of alkyl ammonium species partially passivating the surface states.

While the employment of amines as surface passivants for CdSe has been reported only in the past decade,[64] the original high temperature synthesis of CdSe nanocrystals employed TOPO as the predominant surface ligand.[9] For this reason it has become one of the most studied surface chemistries for CdSe nanocrystals. Upon adsorption of TOPO to the surface, the typical IR signature of the unbound P═O vibrational mode at 1145 cm^{-1} is found to shift to lower wavenumbers and split into several bands.[53,65] This behavior of the P═O band has been typically correlated to the existence of different binding sites at the surface of the CdSe nanocrystals.[53] Our results are in accordance with these previous observations, with two distinct vibrational peaks appearing at 1125 and 1036 cm^{-1} following TOPO adsorption (Figure 4C). In addition, consistent with their high surface binding energy, the TOPO ligands are found to displace the majority of the original pyridine coverage at the surface.

The final surface chemistry that we have investigated here is that based on alkane thiols. The relatively simple IR spectrum observed for octadecanethiol is composed predominantly of aliphatic vibrations with a weak S−H stretch at 2557 cm^{-1} (Figure 4D).[65,66] Following adsorption to the CdSe surface, the S−H stretch is no longer observed (Inset of Figure 4D); this is consistent with the surface binding moiety being that of the thiolate ($-S^-$). Interestingly, despite thiolates being able to strongly coordinate to Cd surface states, we observe residual pyridine signals in our dodecanethiol passivated CdSe nanocrystal samples. This again hints at the strongly selective nature of the surface states that exist on such CdSe nanocrystals.[67]

Having qualitatively analyzed the surface chemistry and identified the complexities associated with each

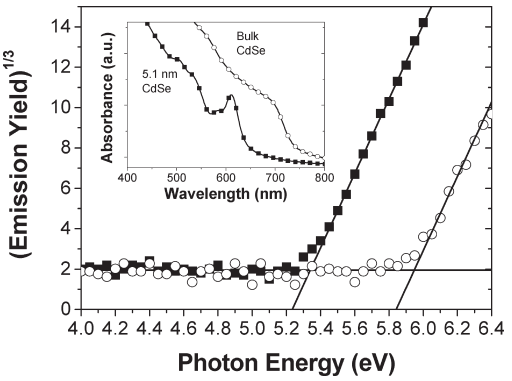

Figure 5. A comparison of the PESA spectrum of 5.1 nm sized CdSe nanocrystals with an alkylamine surface ligand passivation (■) and that of a CdSe nanocrystal thin-film that has been $CdCl_2$ treated and annealed at 400 °C to yield bulk optical characteristics (○). (Inset) The absorption spectra of the quantum confined nanocrystals and the annealed sample showing the bulk-like absorption properties.

ligand type, we are now in a position to study the variation of the ionization energy for CdSe nanocrystals with these various surface chemistries. While our ATR-FTIR studies focused on selective thiols and amines, for the PESA measurements we varied the alkyl chain length sequentially from butyl through to octadecyl for each of these moieties. The mean values of the measured IE for each of the surface chemistries are summarized in Table 1. The variation of the alkyl chain length resulted in no appreciable changes to the IE, with all measurements exhibiting uncorrelated values within ±0.05 eV of the mean. In stark contrast, variation of the surface binding moiety induced changes of up to 0.35 eV. Amine ligands resulted in the lowest IE (5.40 eV) and pyridine overcoated QDs exhibited the highest (5.75 eV). CdSe passivated with TOPO, oleic acid, and thiols exhibited intermediate IEs of 5.45, 5.60, and 5.65 eV, respectively. Despite the shifts of the IE being strongly correlated with the surface binding moiety, variations of up to ±0.05 eV were observed for different nanocrystal samples capped with the same ligand. Both of these observations are in agreement with Soreni-Harari and co-workers who found that for a given surface binding moiety, changes in the overall polarity of the ligand resulted in a lesser variation of the IE than changes to the surface binding moiety itself.[31] Interestingly, through the use of CV, Wang *et al*. found that the reduction potential of CdSe was more negative for octanethiol surface coverages than for TOPO.[23] This is in contradiction to the results found here, suggesting that further verification with another technique may be necessary. Despite this discrepancy, these results indicate the fundamental importance of retaining a similar chemical environment on the surface of QDs when measuring the IE and EA as a function of size.

Studies on bulk CdSe and CdS electrodes have shown that the adsorption of electron donating

ligands or ions on the surface can shift the energy levels by more than 0.5 eV in the cathodic direction.[68] As the major passivating agent in all our studies were Lewis and Brønsted bases, it is expected that in all cases, the energy levels would experience such a shift. To confirm this, we annealed a sample of CdSe nanoparticles at 400 °C following a dip into a saturated $CdCl_2$ solution in methanol. Such a $CdCl_2$ treatment, which is commonly used to induce crystallite growth in CdTe–CdS solar cells,[69,70] causes ligand desorption from the nanocrystals and results in bulk-like absorption with an an optical band gap of close to 1.74 eV—the crystallites typically grow to 30 nm in size as confirmed through X-ray diffraction (see Supporting Information). The IE in this case was 5.9 eV. This bulk value suggests that a cathodic shift of more than 0.5 eV is experienced when primary amines are adsorbed to the surface of CdSe (see Figure 5). Notably, even this value departs from that of an ultraclean CdSe surface which has a reported IE value of 6.6 eV.[71]

The role of surface effects on determining the ionization energy is very complex. However, inspection of the ionization energies presented in Table 1 does hint at a correlation to the hole trapping ability of the surface and/or the ligand. It is well documented that thiolates and pyridine act to efficiently trap holes when adsorbed onto CdSe surfaces.[73] Thiolates, which covalently bind to surface cadmium species, trap holes at the surface through the two lone pairs of electrons on the sulfur. Pyridine, which as we have discussed coordinates CdSe quantum dots mainly through its lone pair on the nitrogen, traps holes away from the surface through a charge transfer from the nanocrystal's bulk or surface to the pyridine's aromatic ring. Much like thiolates, unpassivated selenium surface states can also effectively trap holes.[67,72] To this extent, bulky ligands, such as TOPO,[53] and weak surface binding ligands, such as oleic acid,[59] create a surface that is only partially passivated. This permits hole trapping to occur, *albeit* typically to a lesser extent than in the presence of thiols and pyridine. For CdSe, the small cone angle and the appropriate electrochemistry makes primary amines the best known organic passivants for reducing surface trap densities.[74] Thus, surface hole trapping is less likely to occur in the presence of primary amine than with any other ligand studied here. A qualitative trend can therefore be deduced which suggests that surfaces which are free from hole scavengers and whose surface states are also better passivated, result in a lower ionization energy.

Size-Dependence of the Energy Level Structure in Quantum Dots. Having shown that the surface chemistry of QDs is inherently related to the IE, we are now in a position to study the size-dependence of a variety of different QD materials. In Figure 6 the PESA measured E_{vb} of CdSe, CdTe, PbS, and PbSe QDs as a function of size are shown. To minimize surface variation effects on E_{vb}, great care was taken to ensure the surface chemistries were identical for each particle composition. From the known value of E_{vb}, we used the experimentally determined optical band gaps and eq 5, with the parameters given in Table 2, to determine E_{cb}^{opt}, E_{cb}^{dir}, and E_{cb}. Each of these energy levels are also included in Figure 6. All experimental and calculated data points are tabulated within the Supporting Information, as are full-scale energy level landscapes for each of the quantum dots studied. To establish size-dependent calibration curves for the valence (conduction) band-edge energy levels, the data was fitted to the functional form $E_{vb(cb)}(R) = E_{vb(cb)}(\infty) - (+)AD^{-B}$, where A and B are constants, and D is the nanocrystal diameter. To ensure consistency between the fitted parameters, we utilized the fitting constraint $E_{gap}(\infty) = E_{cb}(\infty) - E_{vb}(\infty)$, where $E_{gap}(\infty)$ is the bulk band gap of the material. These fitting coefficients are summarized in Table 2. For clarity, only the fitted function of E_{cb}^{dir} is included in Figure 6.

To ascertain the validity of the measured energy levels, especially due to the approximations inherent in eq 5, in Figure 6 we include a comparison of data available from various studies on the individual systems. For CdSe QDs, Kucur *et al.*,[21] Inamdar *et al.*,[22] and Querner *et al.*,[75] all studied the size-dependent oxidation and reduction potential properties through cyclic voltammetry. Considering the variation in surface chemistry between these studies, the data show an excellent agreement to that obtained here, *albeit* only when the direct Coulomb interaction and the polarization term are *not* included.

The conduction band-edge shift of CdSe nanocrystals has also been previously studied by Lee *et al*. using X-ray absorption spectroscopy.[76] The authors found that the experimental scaling of the conduction band minimum was proportional to $D^{-0.6}$. In an extension to this work, Meulenberg and co-workers made use of X-ray emission spectroscopy to study the CdSe valence band-edge evolution as a function of size.[77] These authors found that the valence band-edge energy scaled as $D^{-1.6}$. A comparison of the scaling coefficients from these works and that determined here suggests that there is some discrepancy. Standard confinement theory predicts that both conduction and valence band-edge energies should scale as D^{-2}.[17] More sophisticated theories, such as that of SEPM show a reduced scaling coefficient with $E_{cb} \propto D^{-1.3}$ and $E_{vb} \propto D^{-0.95}$. Both of these values are within error of the experimental results presented here. The poor agreement of the X-ray absorption and emission results with our work and the various studies using cyclic voltammetry suggests that the energy values obtained with these techniques need to be further analyzed in order to determine what effects are causing such a large difference to be observed. Lastly, recent studies by the group of Naaman have used low energy photoemission

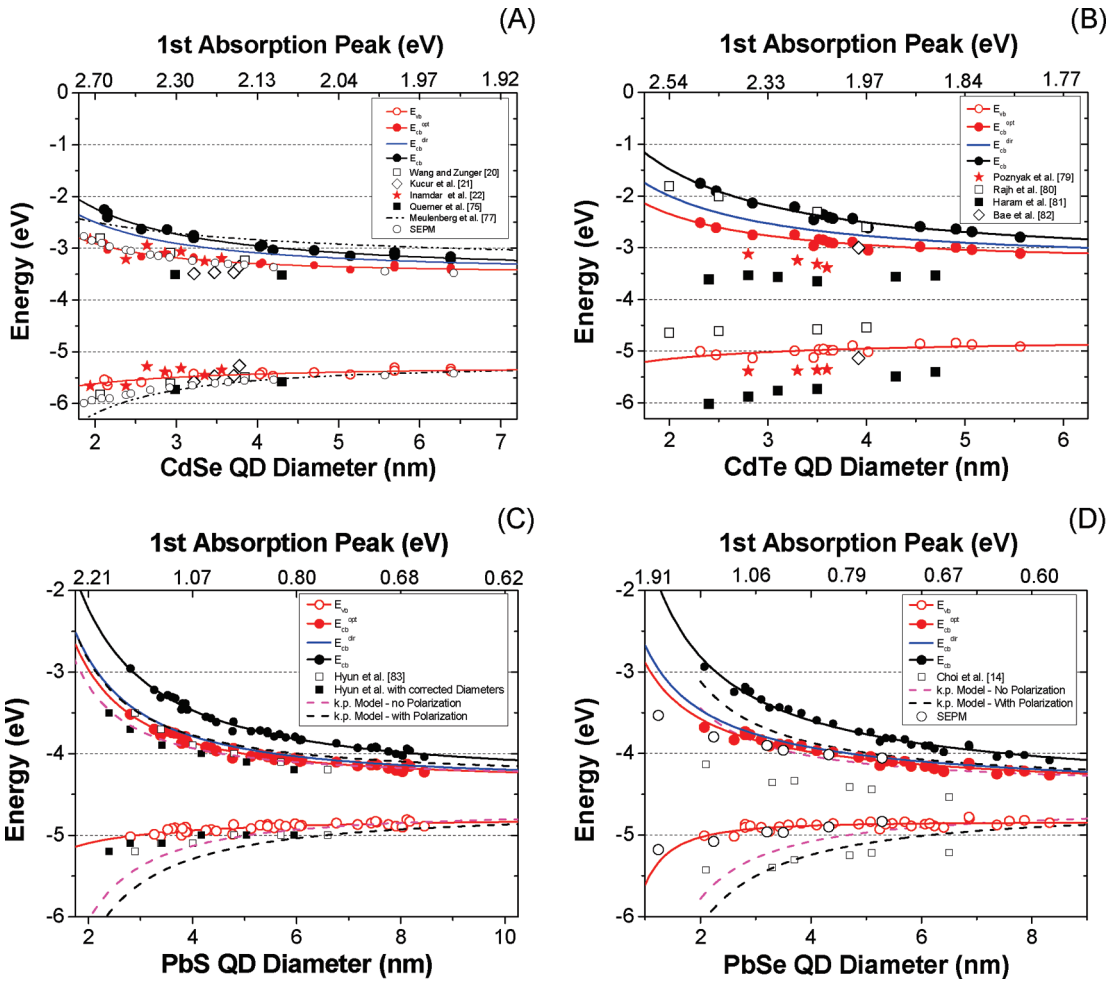

Figure 6. The valence and conduction band-edge energies of (A) CdSe, (B) CdTe, (C) PbS, and (D) PbSe quantum dots as a function of particle diameter (nm) and first absorption energy (eV). The valence band-edge energies, E_{vb}, were determined directly from PESA measurements. The various conduction band-edge energies were calculated from different approximations of eq 5 and are discussed in detail within the text. All energy values were fitted to a power law, with the coefficients of the fits given in Table 2 For clarity, the energy points corresponding to E_{cb}^{dir} have been omitted and only the fitted curve is shown. The results of all systems are compared to available experimental and theoretical literature values from different sources which are referenced within the main text. In addition, we include results from k·p theory for PbS and PbSe, and our own calculations based on SEPM for CdSe and PbSe. Owing to a different optical band gap *versus* size calibration curves employed, we have recalculated the PbS data from Hyun *et al.*[83] to ensure a valid comparison with our own values. Finally, it should be noted that the top *x*-axis (first absorption energy (eV)) of each plot only applies to the experimental data and is correlated to the diameters through known calibration curves (see main text for details).

TABLE 2. Summary of Valence and Conduction Band-Edge Energies for CdSe, CdTe, PbS, and PbSe Quantum Dots[a]

	CdSe	CdTe	PbS	PbSe
ε_{opt}	6.2	7.2	17	23
$E_{g,bulk}$ (ev)	1.74	1.45	0.41	0.28
E_{vb}	$-5.23 - 0.74D^{-0.95}$	$-4.74 - 0.80D^{-0.97}$	$-4.76 - 0.64D^{-0.90}$	$-4.84 - 0.77D^{-2.94}$
E_{cb}^{opt}	$-3.49 + 1.79D^{-1.62}$	$-3.29 + 2.58D^{-1.45}$	$-4.35 + 3.93D^{-1.51}$	$-4.56 + 1.674D^{-0.77}$
E_{cb}^{dir}	$-3.49 + 2.47D^{-1.32}$	$-3.29 + 3.21D^{-1.31}$	$-4.35 + 4.10D^{-1.44}$	$-4.56 + 1.888D^{-0.79}$
E_{cb}	$-3.49 + 2.97D^{-1.24}$	$-3.29 + 4.19D^{-1.21}$	$-4.35 + 5.12D^{-1.27}$	$-4.56 + 3.167D^{-0.86}$

[a] The parameters included within this table include the bulk dielectric constant at optical frequencies (ε_{opt}), the bulk optical band gap ($E_{g,bulk}$), the PESA determined valence band-edge energy (E_{vb}), and the various conduction band-edge energy approximations (E_{cb}^{opt}, E_{cb}^{dir}, and E_{cb}) which are described in detail in the main text.

spectroscopy to study CdSe on gold substrates.[78] For clarity, these results are not shown here, but are in good agreement with the values shown above. Notably, in those studies, the CdSe were chemically linked to gold surfaces, and showed a surface pinning phenomenon. We did not see pinning of the valence-band, presumably because long chained ligands were used and our substrates were not metallic.

While numerous studies are available on the energy level structure of CdSe quantum dots, significantly fewer have focused on CdTe quantum dots. In Figure 6B we show how our experimental data compare to existing studies that were performed by either cyclic voltammetry or differential pulse voltammetry (DPV).[79−82] A good correlation in the trend of the data between these studies and our own is observed; however, the magnitude of the values does show some variation. As we have previously discussed, this factor could arise from surface chemistry differences between samples. Notably, the study by Bae *et al.*[82] who used DPV to measure the true quasi-particle gap is in quantitative agreement with our results. Similarly to that of CdSe, this is only the case when the Coulomb and polarization contributions are *not* considered in defining the conduction band-edge energy.

Finally, the energy levels of PbS and PbSe are compared to those determined by Hyun *et al.*[83] and Choi *et al.*[14] In these works, the authors determined E_{cb} through CV and calculated the E_{vb} from the optical gap. They did not include the direct Coulomb interaction or the polarization contribution in their calculation. To ensure an accurate comparison of these studies to ours, it is important to ensure that the size-dependent calibration curve of the optical band gap is identical. While for PbSe this is the case, the authors used a different calibration for PbS. Thus, for PbS the E_{vb} values were recalculated based on their experimentally determined E_{cb}; these recalculated values are also included in Figure 6C. Despite PESA measuring E_{vb}, a good agreement is observed between both the conduction and valence band-edge energies of PbS QDs, but again only when the polarization interaction is *not* included.

The Coulomb interaction is expected to be extremely small for both PbS and PbSe due to their high dielectric constants.[84] However, the high dielectric mismatch between the QDs and the host matrix should significantly increase the contribution from the surface polarization. Unlike in CV, this is particularly true in our case, where there is no electrolyte to screen charges within the QDs from the dielectric environment. Concordant with all the other QDs studied here, the agreement between our results and those of Hyun *et al.*[83] suggests that the polarization contribution described within eq 5 is negligible in our measurements. Interestingly, while a good agreement for the energy levels of PbS QDs is observed, a significant variation for PbSe nanocrystals is found. At present, we do not understand what causes this variation, particularly as the surface chemistry of the PbSe QDs used in both studies was the same.

Within an infinite surface-barrier confinement (*i.e.,* particle-in-the-box) model, ignoring direct Coulomb interactions and polarization contributions, the relative magnitude of the valence and conduction band-edge energy level shifts are: $\Delta E_{cb}(R)/\Delta E_{vb}(R) \propto m_h^*/m_e^*$, where m^* is the effective mass of the electron (e) and hole (h). On the basis of this simple model, the band which possesses a lower effective charge mass should therefore exhibit a larger energy shift. Our results for both CdSe and CdTe QDs show that the conduction band-edge shifts approximately 3−5 times more than the valence band. This is consistent with the ratio of the electron and hole effective masses of both bulk materials. In the case of PbS and PbSe QDs, one would expect close to equal shifting of both bands due to similar electron and hole effective masses. This is clearly not observed here.

The simplicity of the above analysis makes any comparison qualitative at best. Therefore, to further gauge the validity of the mapped out energy level structures we employed $\mathbf{k}\cdot\mathbf{p}$ theory and SEPM calculations for CdSe, PbS, and/or PbSe quantum dots. Beginning with CdSe, a comparison of our experimental data to the SEPM calculation of Wang and Zunger,[20] as well as our own SEPM results, show a good correlation. It is worth mentioning that neither Wang and Zunger's nor our SEPM calculations include any electron−hole Coulomb (direct or polarization) contribution: the calculated band-edges are separated by $E_{gap}^{0} \approx E_{gap}^{opt} + J_{eh}^{dir}$.[42] The discrepancy between our experimental and theoretical results is indeed of the order of the direct electron−hole Coulomb interaction and decreases with increasing size (see Supporting Information).

The agreement between the experimental trends and the SEPM calculations, confirms the already drawn conclusion from above, that the dielectric confinement does not play a significant role in defining the energy level structures under our experimental conditions and that eventual contributions are within our experimental error. It is worthwhile mentioning that earlier studies on the valence band-edge shift of CdS as studied through UPS did suggest that polarization contributions needed to be included.[25] Further efforts are needed in this area to understand why this was the case.

For the Pb based particles, $\mathbf{k}\cdot\mathbf{p}$ theory was employed as a comparison for both PbS and PbSe quantum dots.[85] In both cases a reasonable agreement is found for the larger particle sizes. However, for smaller sizes an overestimated (underestimated) shift of the valence (conduction) band-edge is predicted. At first glance, this situation could be interpreted as arising from the energy levels being pinned by the surface, a phenomenon that has been observed for CdSe on gold[78] and on ZnO[86] surfaces. In an attempt to further understand the difference between our experimental results and those predicted by $\mathbf{k}\cdot\mathbf{p}$ theory, we performed atomistic SEPM calculations on PbSe nanocrystals of different sizes. The single-particle energy spectrum calculated using SEPM has been shown[84] to be substantially different from that obtained using the

4 × 4 L-centered **k·p** approach by Kang and Wise.[85] In contrast to SEPM, the latter method in fact (i) exaggerates the degree of confinement by assuming unrealistic, infinite potential barriers, (ii) limits the valence-conduction coupling to a single band for each edge, (iii) neglects intervalley coupling, and (iv) inaccurately accounts for the anisotropy of the effective-masses. This leads to an incorrect mirror-symmetrical picture of the conduction and valence band and to the expectation of almost symmetrical size-dependent shifts for the two bands. When effects i−iv are properly accounted for, as in our SEPM calculations, a different picture to that predicted by **k·p** theory emerges.[84,87] Following a realignment of the diameters due to the known mismatch between SEPM and experimentally determined optical-gap *versus* size (based on the calibration curves employed to assign the sizes in our experiments[49]), a remarkably good correlation between the calculated and experimentally observed valence and conduction bands shifts is achieved (see Figure 6).[88] It is worth mentioning that the SEPM energies plotted in Figure 6 do *not* include any electron−hole interaction or surface polarization contribution. The large dielectric mismatch between the QD core and the local environment should result in a substantial contribution to the polarization energy, which, assuming a matrix dielectric constant of ~2 could be as large as 0.4 eV for the smallest PbSe dots considered in our study.[89] This contribution would be reflected in both the conduction and valence band-edge energies. On the basis of the good agreement between our SEPM calculations and the experimentally determined energy levels, it appears that the polarization contribution to the energy level structure is negligible.

A natural question is why does the polarization contribution appear so insignificant in determining the electronic level structure of quantum dots? In an attempt to address this, we highlight that the approximation for the polarization energy provided in eq 5 is a great simplification to the real dielectric properties in our system. The two major factors that are ignored in this approximation are (i) a size dependent quantum dot dielectric constant and (ii) the role of the surface. The slight reduction in the dielectric constant as the particle size decreases would result in a concordant, but slight, decrease to the contribution of the mutual dielectric polarization contribution. The latter factor considers the screening of residual charges within the QDs by either unpassivated surface states or highly polarizable binding moieties at the surface. To the authors' knowledge, the impact of binding moieties on the local dielectric constant has not been previously addressed. Meanwhile, the role of surface states has been probed using density-functional theory on PbSe slabs, suggesting that their existence results in an enhancement of the local dielectric constant at the surface by over 20% compared to the bulk.[47] In both cases, no estimates of the magnitude of such effects on the ionization energies have been reported.

From photoemission spectroscopy of metal clusters, it is known that the energy of a photoelectron is influenced by its interaction with the residual photohole.[90,91] This interaction, which occurs on a femtosecond time scale, was employed by Wu and coworkers to show how the ionization energy in semiconductor nanocrystals can change depending on how rapidly the residual photohole can be neutralized.[32] According to this model, rapid neutralization of the photohole acts to reduce the total interaction energy between the ejected electron and the hole, thereby decreasing the ionization energy. Provided that the magnitude of this decrease is close to that of the polarization contribution, the latter would not be observed. An alternate viewpoint is that instead of the photohole being neutralized, it becomes trapped near or at the surface. Under these conditions, the surface polarization contribution of the hole could potentially diminish.[92] This would actively reduce its contribution to the final ionization energy. In addition, the electron and hole would experience a stronger direct Coulomb interaction, due to the lower dielectric constant provided by the organic ligands and air. An interesting corollary of this effect is that surface chemistries providing a higher rate of hole charge trapping would induce a larger total direct Coulomb interaction between the ejected electron and photohole. This would suggest that for CdSe nanocrystals, ligands which favorably passivated the surfaces (*e.g.*, alkyl amines) would exhibit the lowest ionization energies, while those which actively trapped holes (*e.g.*, thiols and pyridine) would exhibit the highest. Overall, this picture would explain why we do not see the surface polarization contribution of the hole in our measurements and would also account for the origin of the ionization energy dependence of CdSe nanocrystals on surface ligands.

CONCLUSIONS

In this study we have examined the size-dependence of the valence and conduction band-edge energies of CdSe, CdTe, PbS, and PbSe quantum dots through photoelectron spectroscopy in air. The measured valence band-edge energies were compared to previous studies and were found to be in good agreement with SEPM calculations. This was particularly important for PbSe, for which we did not observe a symmetric splitting of the valence and conduction bands as predicted by **k·p** theory. Instead, SEPM calculations, which correctly describe the electronic structures in the valence and conduction bands, could predict the size-dependent trend of the valence and conduction band-edge energies. In addition, while confinement theory predicts that the ionization

energy should include a size-dependent dielectric confinement term, we found that this contribution was negligible for all the nanocrystals studies here. This factor was rationalized through surface contributions and from the final-state effect, which is known to arise from the finite lifetime or surface trapping of the photohole following photoionization. Finally, we used CdSe quantum dots as a test case for studying the effect of changing surface ligands on the ionization energy. We observed that the ionization energy could shift by as much as 0.35 eV through a variation in the surface chemistry, a value that was larger than the energy level shift due to confinement. The trend in the data indicates that surface chemistries which provide greater hole trapping rates induces larger ionization energies. Overall, in this work we have shown how photoelectron spectroscopy in air can be used to map out the energy level structure of quantum confined nanocrystals. This work will pave the way to future studies that attempt to further unravel how the complex interplay between surface and bulk states define the size-dependent optical and electronic properties of quantum confined structures.

METHODS

All chemicals were purchased from Aldrich and solvents from Univar. These were used without further purification.

Quantum Dot Synthesis. CdSe, CdTe, PbS, and PbSe quantum dots of varying size were synthesized under high temperature lyophobic conditions through established protocols.[2,13,93,94] For CdSe and CdTe QDs, the samples were washed twice *via* a chloroform−hexane−methanol−acetone extraction (1:1:4:1 v/v), then precipitated with chloroform/acetone combinations. The nanocrystals were dispersed in chloroform and then ligand exchanged with 5-amino-1-pentanol to induce flocculation. Following centrifugation for 5 min at 4400 rpm, the QD precipitate was dispersed in a chloroform−ethanol mixture (1:1 v/v). For the oleic acid capped PbSe and PbS samples, the QDs in their growth solution were initially precipitated with acetone. The precipitate was washed a further two times from chloroform using acetone as a nonsolvent then dispersed in chloroform.

For the CdSe ligand exchange experiments, the QDs were washed as described above except instead of exchanging the surface with 5-amino-1-pentanol, pyridine was used with hexane as a nonsolvent. The QDs were heated in pyridine at 90 °C for 5 h under nitrogen then precipitated with minimum hexane. This step was repeated. The QDs were redispersed in a solution of chloroform with the corresponding ligand at a concentration corresponding to a 1000−10 000 excess with respect to the total nanocrystal surface states in solution. The ligand exchange process was allowed to take place at 50 °C over 2 h. Precipitation with an appropriate nonsolvent followed (ethanol or acetone), before final dispersion in chloroform.

Samples were prepared for photoelectron measurements by drop casting or spin-coating dilute solutions of QDs onto ITO or borosilicate glass slides to form thin films ranging from 10 to 100 nm in thickness. We found that the choice of substrate or the films thickness in this range did not affect the observed values. Both of these factors indicate that charging was not a concern within these experiments. For ATR-FTIR, samples were drop-cast directly onto the diamond crystal and allowed to dry before carrying out the measurements.

Instrumentation. Absorbance spectra in solution and on thin-films were collected with a Cary 5 UV−vis−NIR spectrometer. Surface analysis was carried out using a Thermo Scientific Nicolet 6700 attenuated total reflectance Fourier transform infrared (ATR-FTIR) spectrometer. PESA measurements were conducted on a Riken Keiki AC-2 photoelectron spectrometer. The error in the ionization energies determined from the PESA measurements on a given sample were ±0.05 eV.

Acknowledgment. J.J. acknowledges the financial support through the CSIRO office of the chief executive postdoctoral fellowship scheme. M.C. gratefully acknowledges the Royal Society for financial support under the URF scheme. The authors would like to thank A. C. Bartnick for useful discussions throughout the preparation of this manuscript and for providing the **k·p** theory predictions for PbS and PbSe quantum dots. Likewise, the authors acknowledge Dr. D. Gómez and Prof. P. Mulvaney for useful discussions and critical reading of the manuscript. This work was supported by the Victorian Organic Solar Cell Consortium.

Supporting Information Available: X-ray diffraction showing the increased size of CdSe crystallites following cadmium chloride treatment and thermal annealing, description of the fitting procedure to determine the ionization energy levels from the photoelectron yield measurements, size-dependent optical band gap relations for the various semiconductors studied, tabulated data of all the energy points, full-page size-dependent energy level diagrams for all nanocrystals, and SEPM calculations showing the influence of Coulomb interactions on the energy level structure for CdSe. This material is available free of charge *via* the Internet at http://pubs.acs.org.

REFERENCES AND NOTES

1. Alivisatos, A. P. Semiconductor Clusters, Nanocrystals, and Quantum Dots. *Science* **1996**, *271*, 933–937.
2. Yu, W. W.; Qu, L. H.; Guo, W.; Peng, X. Experimental Determination of the Extinction Coefficient of CdTe, CdSe, and CdS Nanocrystals. *Chem. Mater.* **2003**, *15*, 2854–2860.
3. Klimov, V. I. Optical Nonlinearities and Ultrafast Carrier Dynamics in Semiconductor Nanocrystals. *J. Phys. Chem. B* **2000**, *104*, 6112–6123.
4. Jasieniak, J.; Smith, L.; van Embden, J.; Mulvaney, P. Re-examination of the Size-Dependent Absorption Properties of CdSe Quantum Dots. *J. Phys. Chem. C* **2009**, *113*, 19468–19474.
5. Leatherdale, C. A.; Woo, W. K.; Mikulec, F. V.; Bawendi, M. G. On the Absorption Cross Section of CdSe Nanocrystal Quantum Dots. *J. Phys. Chem. B* **2002**, *106*, 7619–7622.
6. Efros, A. L.; Rosen, M. The Electronic Structure of Semiconductor Nanocrystals. *Annu. Rev. Mater. Sci.* **2000**, *30*, 475–521.
7. Norris, D. J.; Bawendi, M. G. Measurement and Assignment of the Size-Dependent Optical Spectrum in CdSe Quantum Dots. *Phys. Rev. B* **1996**, *53*, 16338–16346.
8. Spanhel, L.; Haase, M.; Weller, H.; Henglein, A. Photochemistry of Colloidal Semiconductors. 20. Surface Modification and Stability of Strong Luminescing CdS Particles. *J. Am. Chem. Soc.* **1987**, *109*, 5649–5655.
9. Murray, C. B.; Norris, D. J.; Bawendi, M. G. Synthesis and Characterization of Nearly Monodisperse CdE (E = Sulfur, Selenium, Tellurium) Semiconductor Nanocrystallites. *J. Am. Chem. Soc.* **1993**, *115*, 8706–8715.
10. Peng, X.; Manna, L.; Yang, W.; Wickham, J.; Scher, E.; Kadavanich, A.; Alivisatos, A. P. Shape Control of CdSe Nanocrystals. *Nature* **2000**, *404*, 59–61.
11. Murray, C. B.; Sun, S. H.; Gaschler, W.; Doyle, H.; Betley, T. A.; Kagan, C. R. Colloidal Synthesis of Nanocrystals and Nanocrystal Superlattices. *IBM J. Res. Dev.* **2001**, *45*, 47–56.

12. Gur, I.; Fromer, N. A.; Geier, M. L.; Alivisatos, A. P. Air-Stable All-Inorganic Nanocrystal Solar Cells Processed from Solution. *Science* **2005**, *310*, 462–465.
13. Luther, J. M.; Law, M.; Beard, M. C.; Song, Q.; Reese, M. O.; Ellingson, R. J.; Nozik, A. J. Schottky Solar Cells Based on Colloidal Nanocrystal Films. *Nano Lett.* **2008**, *8*, 3488–3492.
14. Choi, J. J.; Lim, Y.-F.; Sentiago-Berrios, M. B.; Oh, M.; Hyun, B.-R.; Sun, L.; Bartnik, A. C.; Goedhart, A.; Malliaras, G. G.; Abruña, H.; *et al*. PbSe Nanocrystal Excitonic Solar Cells. *Nano Lett.* **2009**, *9*, 3749–3755.
15. Konstantatos, G.; Howard, I.; Fischer, A.; Hoogland, S.; Clifford, J.; Klem, E.; Levina, L.; Sargent, E. H. Ultrasensitive Solution-Cast Quantum Dot Photodetectors. *Nature* **2006**, *442*, 180–183.
16. Coe, S.; Woo, W.-K.; Bawendi, M.; Bulovic, V. Electroluminescence from Single Monolayers of Nanocrystals in Molecular Organic Devices. *Nature* **2002**, *420*, 800–803.
17. Brus, L. E. A Simple Model for the Ionization Potential, Electron Affinity, and Aqueous Redox Potentials of Small Semiconductor Crystallites. *J. Chem. Phys.* **1983**, *79*, 5566–5571.
18. Lippens, P. E.; Lannoo, M. Comparison between Calculated and Experimental Values of the Lowest Excited Electronic State of Small CdSe Crystallites. *Phys. Rev. B* **1990**, *41*, 6079–6081.
19. Wang, L.-W.; Li, J. First-Principles Thousand-Atom Quantum Dot Calculations. *Phys. Rev. B* **2004**, *69*, 153302.
20. Wang, L.-W.; Zunger, A. Pseudopotential Calculations of Nanoscale CdSe Quantum Dots. *Phys. Rev. B* **1996**, *53*, 9579–9582.
21. Kucur, E.; Riegler, J.; Urban, G. A.; Nann, T. Determination of Quantum Confinement in CdSe Nanocrystals by Cyclic Voltammetry. *J. Chem. Phys.* **2003**, *119*, 2333–2337.
22. Inamdar, S. N.; Ingole, P. P.; Haram, S. K. Determination of Band Structure Parameters and the Quasi-particle Gap of CdSe Quantum Dots by Cyclic Voltammetry. *ChemPhysChem* **2008**, *9*, 2574–2579.
23. Wang, C.; Shim, M.; Guyot-Sionnest, P. Electrochromic Nanocrystal Quantum Dots. *Science* **2001**, *291*, 2390–2392.
24. Wehrenberg, B. L.; Guyot-Sionnest, P. Electron and Hole Injection in PbSe Quantum Dot Films. *J. Am. Chem. Soc.* **2003**, *125*, 7806–7807.
25. Colvin, V. L.; Alivisatos, A. P.; Tobin, J. G. Valence-Band Photoemission from a Quantum-Dot System. *Phys. Rev. Lett.* **1991**, *66*, 2786–2789.
26. van Buuren, T.; Dinh, L. N.; Chase, L. L.; Siekhaus, W. J.; Terminello, L. J. Changes in the Electronic Properties of Si Nanocrystals as a Function of Particle Size. *Phys. Rev. Lett.* **1998**, *80*, 3803–3806.
27. Munro, A. M.; Zacher, B.; Graham, A.; Armstrong, N. R. Photoemission Spectroscopy of Tethered CdSe Nanocrystals: Shifts in Ionization Potential and Local Vacuum Level as a Function of Nanocrystal Capping Ligand. *ACS Appl. Mater. Interfaces* **2010**, *2*, 863–869.
28. Hwang, J.; Wan, A.; Kahn, A. Energetics of Metal–Organic Interfaces: New Experiments and Assessment of the Field. *Mater. Sci. Eng. R* **2009**, *64*, 1–31.
29. Yi, Y.; Lyon, J. E.; Beerbom, M. M.; Schlaf, R. Characterization of Indium Tin Oxide Surfaces and Interfaces Using Low Intensity X-ray Photoemission Spectroscopy. *J. Appl. Phys.* **2006**, *100*, 093719.
30. D'Andrade, B. W.; Datta, S.; Forrest, S. R.; Djurovich, P.; Polikarpov, E.; Thompson, M. E. Relationship between the Ionization and Oxidation Potentials of Molecular Organic Semiconductors. *Org. Electron.* **2005**, *6*, 11–20.
31. Soreni-Harari, M.; Yaacobi-Gross, N.; Steiner, D.; Aharoni, A.; Banin, U.; Millo, O.; Tessler, N. Tuning Energetic Levels in Nanocrystal Quantum Dots through Surface Manipulations. *Nano Lett.* **2008**, *8*, 678–684.
32. Wu, P.-J.; Tsuei, K.-D.; Hsieh, M.-T.; Wei, K.-H.; Liang, K. S. Dependence of the Final-State Effect on the Coupling between a CdSe Nanoparticle and its Neighbors Studied with Photoemission Spectroscopy. *Phys. Rev. B* **2007**, *75*, 115402.
33. Uda, M. Open Counter for Low Energy Electron Detection. *Jpn. J. Appl. Phys.* **1985**, *24*, 284–288.
34. Uda, M.; Nakagawa, Y.; Yamamoto, T.; Kawasaki, M.; Nakamura, A.; Saito, T.; Hirose, K. Successive Change in Work Function of Al Exposed to Air. *J. Electron. Spectrosc.* **1998**, *88–91*, 767–771.
35. Onoda, M.; Tada, K.; Nakayama, H. Electronic Energy States of Organic Interfaces Studied by Low-Energy Ultraviolet Photoemission Spectroscopy. *J. Appl. Phys.* **1999**, *86*, 2110–2215.
36. Davis, R. J.; Lloyd, M. T.; Ferreira, S. R.; Bruzek, M. J.; Watkins, S. E.; Lindell, L.; Sehati, P.; Fahlman, M.; Anthony, J. E.; Hsu, J. W. P. Determination of Energy Level Alignment at Interfaces of Hybrid and Organic Solar Cells Under Ambient Environment. *J. Mater. Chem.* **2011**, *21*, 1721–1729.
37. Winzenberg, K. N.; Kemppinen, P.; Fanchini, G.; Bown, M.; Collis, G. E.; Forsyth, C. M.; Hegedus, K.; Singh, Th. B.; Watkins, S. E. Dibenzo[b,def]chrysene Derivatives: Solution-Processable Small Molecules that Deliver High Power-Conversion Efficiencies in Bulk Heterojunction Solar Cell. *Chem. Mater.* **2009**, *21*, 5701–5703.
38. Eastman, D. E. Photoelectric Work Functions of Transition, Rare-Earth, and Noble Metals. *Phys. Rev. B* **1970**, *2*, 1–2.
39. For metals and degenerately doped semiconductors, the ionization energy is equivalent to the work function.
40. Kane, E. O. Theory of Photoelectric Emission from Semiconductors. *Phys. Rev.* **1962**, *127*, 131–141.
41. Gobeli, G. W.; Allen, F. G. Direct and Indirect Excitation Processes in Photoelectric Emission from Silicon. *Phys. Rev.* **1962**, *127*, 141–149.
42. Franceschetti, A.; Zunger, A. Pseudopotential Calculations of Electron and Hole Addition spectra of InAs, InP, and Si quantum dots. *Phys. Rev. B* **2000**, *62*, 2614–2623.
43. Banin, U.; Cao, Y.; Katz, D.; Millo, O. Identification of Atomic-like Electronic States in Indium Arsenide Nanocrystal Quantum Dots. *Nature* **1999**, *400*, 542–544.
44. Brus, L. E. Electron–Electron and Electron–Hole Interactions in Small Semiconductor Crystallites: The Size Dependence of the Lowest Excited Electronic State. *J. Chem. Phys.* **1984**, *80*, 4403–4409.
45. Drndić, M.; Jarosz, M. V.; Morgan, N. Y.; Kastner, M. A.; Bawendi, M. G. Transport Properties of Annealed CdSe Colloidal Nanocrystal Solids. *J. Appl. Phys.* **2002**, *92*, 7498–7503.
46. Alves-Santos, M.; Di Felice, R.; Goldoni, G. Dielectric Functions of Semiconductor Nanoparticles from the Optical Absorption Spectrum: The Case of CdSe and CdS. *J. Phys. Chem. C* **2010**, *114*, 3776–3780.
47. Moreels, I.; Allan, G.; De Geyter, B.; Wirtz, L.; Delerue, C.; Hens, Z. Dielectric Function of Colloidal Lead Chalcogenide Quantum Dots Obtained by a Kramers–Krönig Analysis of the Absorbance Spectrum. *Phys. Rev. B* **2010**, *81*, 235319.
48. Cademartiri, L.; Montanari, E.; Calestani, G.; Migliori, A.; Guagliardi, A.; Ozin, G. A. Size-Dependent Extinction Coefficients of PbS Quantum Dots. *A. J. Am. Chem. Soc.* **2006**, *128*, 10337–10346.
49. Moreels, I.; Lamber, K.; De Muynck, D.; Vanhaecke, F.; Poelman, D.; Martins, J. C.; Allan, G.; Henz, Z. Composition and Size-Dependent Extinction Coefficient of Colloidal PbSe Quantum Dots. *Chem. Mater.* **2007**, *19*, 6101–6106.
50. Corrsin, L.; Fax, B. J.; Lord, R. C. The Vibrational Spectra of Pyridine and Pyridine-d_5. *J. Chem. Phys.* **1953**, *21*, 1170–1176.
51. DiLella, D. P.; Stidham, H. D. Vibrational Spectra of C_{2v} Deuterium-Substituted Pyridines. *J. Raman Spectrosc.* **1980**, *9*, 90–106.
52. Long, D. A.; Thomas, E. L. Spectroscopic and Thermodynamic Studies of Pyridine Compounds. *Trans. Faraday Soc.* **1963**, *59*, 783–791.
53. Bowen Katari, J. E.; Colvin, V. L.; Alivisatos, A. P. X-ray Photoelectron-Spectroscopy of CdSe Nanocrystals with Applications to Studies of the Nanocrystal Surface. *J. Phys. Chem.* **1994**, *98*, 4109–4117.

54. Haq, S.; King, D. A. Configurational Transitions of Benzene and Pyridine Adsorbed on Pt{111} and Cu{110} Surfaces: An Infrared Study. *J. Phys. Chem.* **1996**, *100*, 16957–16965.
55. Huo, S.-J.; Xue, X.-K.; Yan, Y.-G.; Li, Q.-X.; Ma, M.; Cai, W.-B.; Xu, Q.-J.; Osawa, M. Extending *in Situ* Attenuated-Total-Reflection Surface-Enhanced Infrared Absorption Spectroscopy to Ni Electrodes. *J. Phys. Chem. B* **2006**, *110*, 4162–4169.
56. Zaki, M. I.; Hasan, M. A.; Al-Sagheer, F. A.; Pasupulety, L. *In Situ* FTIR Spectra of Pyridine Adsorbed on $SiO_2-Al_2O_3$, TiO_2, ZrO_2 and CeO_2: General Considerations for the Identification of Acid Sites on Surfaces of Finely Divided Metal Oxides. *Colloid Surf., A* **2001**, *190*, 261–274.
57. Ji, X.; Copenhaver, D.; Sichmeller, C.; Peng, X. Ligand Bonding and Dynamics on Colloidal Nanocrystals at Room Temperature—The Case of Alkylamines on CdSe Nanocrystals. *J. Am. Chem. Soc.* **2008**, *130*, 5726–5735.
58. Wu, N.; Fu, L.; Su, M.; Aslam, M.; Wong, K. C.; Dravid, V. P. Interaction of Fatty Acid Monolayers with Cobalt Nanoparticles. *Nano Lett.* **2004**, *4*, 383–386.
59. Puzder, A.; Williamson, A. J.; Zaitseva, N.; Galli, G.; Manna, L.; Alivisatos, A. P. The Effect of Organic Ligand Binding on the Growth of CdSe Nanoparticles Probed by *ab Initio* Calculations. *Nano Lett.* **2004**, *4*, 2361–2365.
60. Mui, C.; Han, J. H.; Wang, G. T.; Musgrave, C. B.; Bent, S. F. Proton Transfer Reactions on Semiconductor Surfaces. *J. Am. Chem. Soc.* **2002**, *124*, 4027–4038.
61. Zhang, J. L.; Srivastava, R. S.; Misra, R. D. K. Core–Shell Magnetite Nanoparticles Surface Encapsulated with Smart Stimuli-Responsive Polymer: Synthesis, Characterization, and LCST of Viable Drug-Targeting Delivery System. *Langmuir* **2007**, *23*, 6342–6351.
62. Haigh, J. M.; Van Dam, M. A.; Thornton, D. A. Infrared Evidence for the Trasmission of Electronic Effects through a Metal Atom in a Series of New Cadmium Complexes. *Z. Anorg. Allg. Chem.* **1967**, *355*, 94–103.
63. Vollhardt, D.; Wittig, M.; Petrov, J. G.; Malewski, G. Infrared Spectroscopic Study of Phosphate Counter Ions Bonded in Skimmed Monolayers and Transferred Multilayers of Octadecylamine. *Colloid Polym. Sci.* **1985**, *106*, 28–32.
64. Talapin, D. V.; Rogach, A. L.; Kornowski, A.; Haase, M.; Weller, H. Highly Luminescent Monodisperse CdSe and CdSe/ZnS Nanocrystals Synthesized in a Hexadecylamine–Trioctylphosphine Oxide–Trioctylphospine Mixture. *Nano Lett.* **2001**, *1*, 207–211.
65. von Holt, B.; Kudera, S.; Weiss, A.; Schrader, T. E.; Manna, L.; Parak, W. J.; Braun, M. Ligand Exchange of CdSe Nanocrystals Probed by Optical Spectroscopy in the Visible and Mid-IR. *J. Chem. Mater.* **2008**, *18*, 2728–2732.
66. Eilon, M. J.; Mokari, T.; Banin, U. Surface Exchange Effect on Hyper Rayleigh Scattering in CdSe Nanocrystals. *J. Phys. Chem.* **2001**, *105*, 12726–12731.
67. Jasieniak, J.; Mulvaney, P. From Cd-Rich to Se-Rich—The Manipulation of CdSe Nanocrystal Surface Stoichiometry. *J. Am. Chem. Soc.* **2007**, *129*, 2841–2848.
68. Natan, M. J.; Thackeray, J. W.; Wrighton, M. S. Interaction of Thiols with *n*-Type Cadmium Sulfide and *n*-Type Cadmium Selenide in Aqueous Solutions: Adsorption of Thiolate Anion and Efficient Photoelectrochemical Oxidation to Disulfides. *J. Phys. Chem.* **1986**, *90*, 4089–4098.
69. Romeo, N.; Bosio, A.; Tedeschi, R.; Romeo, A.; Canevari, V. A Highly Efficient and Stable CdTe/CdS Thin Film Solar Cell. *Sol. Energy Mater. Sol. C* **1999**, *58*, 209–218.
70. Jasieniak, J.; MacDonald, B. I.; Watkins, S. E.; Mulvaney, P. Solution-Processed Sintered Nanocrystal Solar Cells *via* Layer-by-Layer Assembly. *Nano Lett.* published online, May 27, 2011, http://dx.doi.org/10.1021/nl201282v.
71. Nethercot, A. H., Jr. Prediction of Fermi Energies and Photoelectric Thresholds Based on Electronegativity Concepts. *Phys. Rev. Lett.* **1974**, *33*, 1088–1091.
72. Leung, K.; Whaley, K. B. Surface Relaxation in CdSe Nanocrystals. *J. Chem. Phys.* **1999**, *110*, 11012–11022.
73. Guyot-Sionnest, P.; Shim, M.; Matranga, C.; Hines, M. Intraband Relaxation in CdSe Quantum Dots. *Phys. Rev. B* **1999**, *60*, R2181–2184.
74. Bullen, C.; Mulvaney, P. The Effects of Chemisorption on the Luminescence of CdSe Quantum Dots. *Langmuir* **2006**, *22*, 3007–3013.
75. Querner, C.; Reiss, P.; Sadki, S.; Zegorska, M.; Pron, A. Size and Ligand Effects on the Electrochemical and Spectroelectrochemical Responses of CdSe Nanocrystals. *Phys. Chem. Chem. Phys.* **2005**, *7*, 3204–3209.
76. Lee, J. R. I.; Meulenberg, R. W.; Hanif, K. M.; Mattoussi, H.; Klepeis, J. E.; Terminello, L. J.; van Buuren, T. Experimental Observation of Quantum Confinement in the Conduction Band of CdSe Quantum Dots. *Phys. Rev. Lett.* **2007**, *98*, 146803.
77. Meulenberg, R. W.; Lee, J. R. I.; Wolcott, A.; Zhang, J. Z.; Terminello, L. J.; van Buuren, T. Determination of the Exciton Binding Energy in CdSe Quantum Dots. *ACS Nano* **2009**, *3*, 325–330.
78. Markus, T. Z.; Wu, M.; Wang, L.; Waldeck, D. H.; Oron, D.; Naaman, R. Electronic Structure of CdSe Nanoparticles Adsorbed on Au Electrodes by an Organic Linker: Fermi Level Pinning of the HOMO. *J. Phys. Chem. C* **2009**, *113*, 14200–14206.
79. Poznyak, S. K.; Osipovich, N. P.; Shavel, A.; Talapin, D. V.; Gao, M.; Eychmueller, A.; Gaponik, N. Size-Dependent Electrochemical Behavior of Thiol-Capped CdTe Nanocrystals in Aqueous Solution. *J. Phys. Chem. B* **2005**, *109*, 1094–1100.
80. Rajh, T.; Micic, O. I.; Nozik, A. J. Synthesis and Characterization of Surface-Modified Colloidal CdTe Quantum Dots. *J. Phys. Chem.* **1993**, *97*, 11999–12003.
81. Haram, S. K.; Kshirsagar, A.; Gujarathi, Y. D.; Ingole, P. P.; Nene, O. A.; Markad, G. B.; Nanavati, S. P. Quantum Confinement in CdTe Quantum Dots: Investigation through Cyclic Voltammetry Supported by Density Functional Theory (DFT). *J. Phys. Chem. C* **2011**, *115*, 6243–6249.
82. Bae, Y.; Myung, N.; Bard, A. J. Electrochemistry and Electrogenerated Chemiluminescence of CdTe Nanoparticles. *Nano Lett.* **2004**, *4*, 1153–1161.
83. Hyun, B.-R.; Zhong, Y.-W.; Bartnik, A. C.; Sun, L.; Abruña, H. D.; Wise, F. W.; Goodreau, J. D.; Matthews, J. R.; Leslie, T. M.; Borrelli, N. F. Electron Injection from Colloidal PbS Quantum Dots into Titanium Dioxide Nanoparticles. *ACS Nano* **2008**, *2*, 2206–2212.
84. An, J. M.; Franceschetti, A.; Dudiy, S. V.; Zunger, A. The Peculiar Electronic Structure of PbSe Quantum Dots. *Nano Lett.* **2006**, *6*, 2728–2735.
85. Kang, I.; Wise, F. W. Electronic Structure and Optical Properties of PbS and PbSe Quantum Dots. *J. Opt. Soc. Am. B* **1997**, *14*, 1632–1646.
86. Carlson, B.; Leschkies, K.; Aydil, E. S.; Zhu, X.-Y. Valence Band Alignment at Cadmium Selenide Quantum Dot and Zinc Oxide $(10\bar{1}0)$ Interfaces. *J. Phys. Chem. C* **2008**, *112*, 8419–8423.
87. An, J. M.; Califano, M.; Franceschetti, A.; Zunger, A. Excited-State Relaxation in PbSe Quantum Dots. *J. Chem. Phys.* **2008**, *128*, 164720.
88. As the pseudopotentials used for PbSe were not fitted to the bulk ionization energy, the calculated position of the valence band-edge with respect to the vacuum level is meaningless for this material: it was determined by rigidly shifting *all* our calculated single-particle energies by the *same* amount $\delta\varepsilon$, obtained as the best fit to experiment for the largest theoretical size considered. However the main features in the theoretical results presented in Figure 6D, *i.e.*, the size-dependent shifts of both conduction and valence band and their separation, have not been affected by this shift.
89. An, J. M.; Franceschetti, A.; Zunger, A. Electron and Hole Addition Energies in PbSe Quantum Dots. *Phys. Rev. B* **2007**, *76*, 045401.
90. Wertheim, G. K.; DiCenzo, S. B.; Youngquist, S. E. Unit Charge on Supported Gold Clusters in Photoemission Final State. *Phys. Rev. Lett.* **1983**, *51*, 2310–2313.
91. Hövel, H.; Grimm, B.; Pollmann, M.; Reihl, B. Cluster–Substrate Interaction on a Femtosecond Time Scale Revealed by a High-Resolution Photoemission Study of the Fermi-Level Onset. *Phys. Rev. Lett.* **1998**, *81*, 4608–4611.

92. Bányai, L.; Gilliot, P.; Hu, Y. Z.; Koch, S. W. Surface-Polarization Instabilities of Electron−Hole Pairs in Semiconductor Quantum Dots. *Phys. Rev. B* **1992**, *45*, 14136–14142.
93. van Embden, J.; Mulvaney, P. Nucleation and Growth of CdSe Nanocrystals in a Binary Ligand System. *Langmuir* **2005**, *21*, 10226–10223.
94. Hines, M. A.; Scholes, G. D. Colloidal PbS Nanocrystals with Size-Tunable Near-Infrared Emission: Observation of Post-synthesis Self-Narrowing of the Particle Size Distribution. *Adv. Mater.* **2003**, *15*, 1844–1849.